IRE1 endoribonuclease signaling promotes myeloid cell infiltration in glioblastoma

Joanna Obacz, Jérôme Archambeau, Elodie Lafont, Manon Nivet, Sophie Martin, Marc Aubry, Konstantinos Voutetakis, Raphaël Pineau, Rachel Boniface, Daria Sicari, et al.

IRE1 endoribonuclease signaling promotes myeloid cell infiltration in glioblastoma

Joanna Obacz[1,2], Jérôme Archambeau[1,2], Elodie Lafont[1,2], Manon Nivet[1,2], Sophie Martin[1,2], Marc Aubry[1], Konstantinos Voutetakis[3,4], Raphael Pineau[1,2], Rachel Boniface[1], Daria Sicari[1,2], Diana Pelizzari-Raymundo[1,2], Gevorg Ghukasyan[5], Eoghan McGrath[1,2], Efstathios-Iason Vlachavas[6], Matthieu Le Gallo[1,2], Pierre Jean Le Reste[1,2,7], Kim Barroso[8,9,10,11], Tanya Fainsod-Levi[12], Akram Obiedat[13], Zvi Granot[12], Boaz Tirosh[13], Juhi Samal[14], Abhay Pandit[14], Luc Négroni[8,9,10,11], Nicolas Soriano[1,15], Annabelle Monnier[1], Jean Mosser[1], Aristotelis Chatziioannou[3,6], Véronique Quillien[1,2], Eric Chevet[1,2] and Tony Avril[1,2]

[1]INSERM U1242, Rennes, France. [2]Centre Eugène Marquis, Rennes. [3]ICB, NHRF, Athens, Greece. [4]Department of Biochemistry and Biotechnology, Larissa, Greece. [5]Biosit H2P2, Rennes. [6]e-NIOS PC, Kallithea-Athens. [7]Hospital of St Malo, France. [8]IGBMC, Illkirch, France. [9]CNRS UMR7104, Illkirch. [10]INSERM U1258, Illkirch. [11]Université de Strasbourg, France. [12]Department of Developmental Biology and Cancer Research, Hebrew University of Jerusalem, Israel. [13]IDR, Hebrew University of Jerusalem. [14]CÚRAM, Ireland. [15]CNRS UMR6290, Rennes.

Corresponding author: Tony Avril, Centre Eugène Marquis, Avenue de la bataille Flandres Dunkerque, 35042 RENNES. Email: t.avril@rennes.unicancer.fr

Competing Interests

EC is founder of Thabor Therapeutics (www.thabor-tx.com). The other authors declare no conflicting interests.

Abstract

Background: Intrinsic or environmental stresses trigger the accumulation of improperly folded proteins in the endoplasmic reticulum (ER), leading to ER stress. To cope with this, cells have evolved an adaptive mechanism named the unfolded protein response (UPR) which is hijacked by tumor cells to develop malignant features. Glioblastoma (GB), the most aggressive and lethal primary brain tumor, relies on UPR to sustain growth. We recently showed that IRE1 alpha (referred to IRE1 hereafter), one of the UPR transducers, promotes GB invasion, angiogenesis and infiltration by macrophage. Hence, high tumor IRE1 activity in tumor cells predicts worse outcome. Herein, we characterized the IRE1-dependent signaling that shapes the immune microenvironment towards monocytes/macrophages and neutrophils. *Methods:* We used human and mouse cellular models in which IRE1 was genetically or pharmacologically invalidated and which were tested in vivo. Publicly available datasets from GB patients were also analyzed to confirm our findings. *Results:* We showed that IRE1 signaling, through both the transcription factor XBP1s and the regulated IRE1-dependent decay (RIDD) controls the expression of the ubiquitin-conjugating E2 enzyme UBE2D3. In turn, UBE2D3 activates the NFκB pathway, ensuing chemokine production and myeloid infiltration in tumors. *Conclusion:* Our work identifies a novel IRE1/UBE2D3 pro-inflammatory axis that plays an instrumental role in GB immune regulation.

Key words: glioblastoma, ER stress, IRE1, chemokines, inflammation.

Key points:

- Glioblastoma IRE1 activity promotes myeloid recruitment via chemokine expression
- UBE2D3, a novel component of IRE1/XBP1s/RIDD signaling, controls NFκB activation
- UBE2D3 controls glioblastoma myeloid cell infiltration *in vivo*

Importance of the Study

Glioblastoma aggressiveness partly owes its dismal prognosis to the presence of a tumor supportive microenvironment. Indeed, stromal cells including microglial cells and macrophages promote GB growth. This study stems from our initial observation that the activation of the ER stress sensor IRE1 in GB cells controls the recruitment of host's immune cells (macrophages and microglial cells mainly). However, the precise mechanisms by which IRE1 exerts this function remain unclear. Herein, we dissected the pathways responsible for these proinflammatory signals. We found that UBE2D3, a novel target of IRE1/XBP1s/RIDD signaling, controls NFκB activation in GB cells and the subsequent myeloid infiltration in vivo via chemokine expression. Targeting IRE1 signaling might impede GB aggressiveness, not only by reducing tumor cell invasion and angiogenesis, but also by neutralizing the pro-tumoral inflammation. This study opens a new avenue for therapeutic approaches to improve the efficacy of current treatments.

Graphical abstract

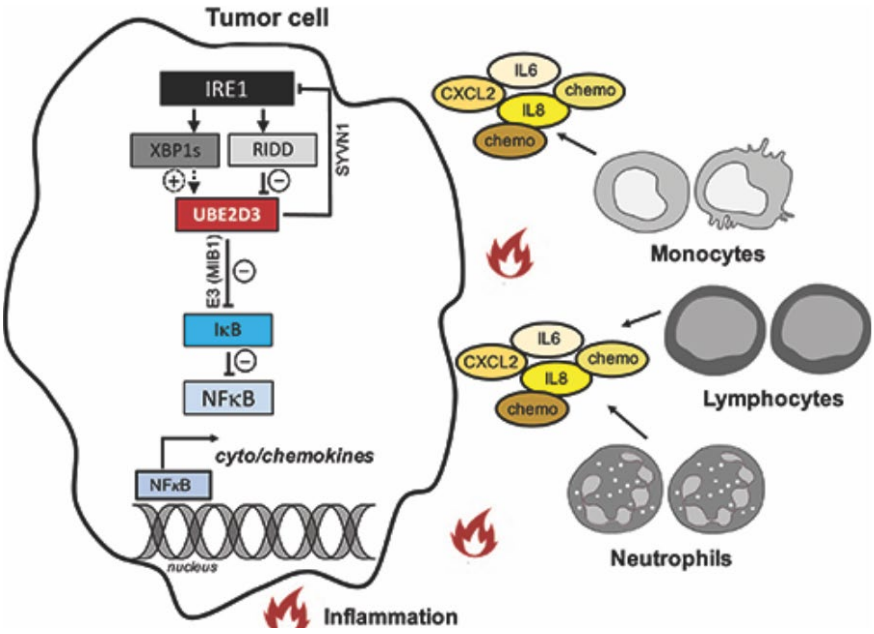

Introduction

Perturbation of ER protein homeostasis is one of the hallmarks of highly proliferative and/or secretory cells. Moreover, many intrinsic and environmental conditions, such as low oxygen levels, acidification or nutrients shortage also increase the risk of misfolded proteins accumulation in the ER lumen, leading to ER stress. To cope with the latter, cells use the UPR which is transduced by the ER transmembrane proteins PERK, ATF6 and the most conserved UPR sensor IRE1 alpha (referred to as IRE1 hereafter). The UPR restores ER homeostasis or induce apoptosis when stress cannot be resolved[1]. Once activated, IRE1, which harbors cytosolic kinase and ribonuclease (RNase) activities, dimerizes/oligomerizes, thus inducing the activation of JNK1, XBP1 mRNA splicing (XBP1s) and Regulated IRE1-dependent decay (RIDD) of RNA[2]. XBP1s activates the transcription of genes involved in protein glycosylation, ER-associated degradation, protein folding, and lipid synthesis. RIDD also controls cell fate under ER stress[3]. The UPR has emerged as an adaptive mechanism supporting tumor progression and resistance to treatment by impacting almost all cancer hallmarks[4]. Mounting evidence also suggests that the UPR shapes the tumor microenvironment by regulating angiogenesis, inflammation and immune response[5,6].

The consequences of UPR signaling have been studied in various cancers such as breast, liver, lung, prostate, pancreas cancers and in GB, the most lethal and aggressive primary brain tumors. IRE1 contributes to GB development by regulating tumor growth, invasion and vascularization[7,8]. Loss of IRE1 signaling also results in decreased expression of proangiogenic and proinflammatory VEGFA, IL1β, IL6, and IL8 in GB cells[8]. Importantly, we have shown a pivotal role of IRE1 in the immune remodeling of GB stroma, which mostly depends on XBP1s[9,10]. However, the precise IRE1-dependent mechanisms by which pro-tumoral inflammation/immune responses are regulated in GB remain elusive. IRE1 signaling induces the expression of proinflammatory chemokines in various models through XBP1s and JNK-dependent pathways or through GSK3β induction. IRE1 also interacts with TRAF2, recruiting IκB kinases (IKK), to promote the degradation of IκB thereby enabling NFκB nuclear

translocation[11]. Since brain tumors are infiltrated by a large number of immune cells, which modulate GB aggressiveness and response to treatment, we aimed here to investigate the molecular mechanisms by which IRE1 controls GB tumor infiltration by immune/inflammatory cells. We showed that IRE1 governs myeloid cell recruitment to GB. This involves a novel IRE1/UBE2D3/NFκB signaling axis, thereby leading to proinflammatory chemokine production and the subsequent recruitment of immune/inflammatory cells to the tumor site.

Materials and Methods

Antibodies and other reagents – Primary antibodies are listed in **Table S1**. Secondary antibodies used were horseradish peroxidase conjugated polyclonal goat anti-rabbit IgG, goat anti-mouse IgG and rabbit anti-goat IgG (all from Dako). Unless specified, all other reagents were from Sigma Aldrich.

Cell culture and treatments – The U87, U87 IRE1.NCK DN cells (referred to as U87 DN), U251 and GL261 lines (all from ATCC) were grown in DMEM medium (Invitrogen) supplemented with 10% fetal bovine serum (FBS) (Lonza) in a 5% CO_2 humidified atmosphere at 37°C. Primary GB lines were previously described[10,12].

Generation of stable cell lines – For stable overexpression of UBE2D3, RADH87 and GL261 cells were transfected with 3µg of pCMV3-UBE2D3-Flag plasmid using Lipofectamine LTX and 2000, respectively (ThermoFisher), following the manufacturer's protocol. For stable ube2d3-downexpression, GL261 cells were transfected with 1µg of pRS shRN-ube2d3. Transfections of GB lines with IRE1 WT and Q780* constructs[10] were performed using Lipofectamine LTX (ThermoFisher), according to the manufacturer's instructions. IRE1 WT and Q780* overexpressing cells were selected using puromycin (ThermoFisher).

Quantitative real-time PCR – Total RNA was extracted using the TRIzol reagent (Invitrogen). RNAs were reverse-transcribed with Maxima Reverse Transcriptase (ThermoFisher), according to the manufacturer's protocol. qPCR was performed with a QuantStudio™ 5 Real-Time PCR System and the PowerUp™ SYBR Green Master Mix (ThermoFisher). Experiments were performed at least in triplicate for each data point. Each sample was normalized based on the expression of the GAPDH or ACTB gene using the $2^{\Delta\Delta CT}$-method. Primers pairs are listed in **Table S2**.

Gel shift assay – Gel shift assay was performed using the LightShift Chemiluminescent EMSA Kit (ThermoFisher) according to the manufacturer's instructions. Biotin end-labeled probes were prepared by PCR using 5' Biotin labeled primers (**Table S3**).

Flow cytometry analyses – Cells were washed in PBS 2% FBS and incubated with saturating concentrations of human immunoglobulins and fluorescent-labelled primary antibodies as indicated for 30 minutes at 4°C. Cells were then washed with PBS 2% FBS and analyzed using a FACSCanto and Novocyte flow cytometers (BD Biosciences and Acea Biosciences).

Myeloid chemoattraction assay – Myeloid cells were washed in DMEM and placed in 3 µm Boyden chambers (Merck Millipore), at 0.5 x 10^5 cells/chamber in 200 µL DMEM. Chambers were simultaneously placed in 500 µL of either control DMEM or tumor cell-conditioned media, and incubated for 2 hours (for PMN) or 16 hours (for Mo) at 37°C. Migrated myeloid cells (under the Boyden chambers) were analyzed by flow cytometry.

Detailed methods are in the Supplemental Materials and Methods. This study does not include any data deposited in external repositories.

Results

Myeloid cells are recruited to GB in an IRE1-dependent manner

We previously demonstrated that IRE1 activity in GB cells controls the recruitment of inflammatory cells such as macrophages and microglial cells[10]. Herein, we tested whether this also applied to other immune cells from the myeloid or lymphoid lineages. To this end, we first investigated whether immune gene signatures were associated with IRE1 activity[10] using the TCGA GB datasets. These immune gene signatures characterize microglia/macrophages (MM) (i.e. blood monocytes-derived macrophages (MDM), microglia cells (MG)[13–15]); polymorphonuclear neutrophils (PMN) and T cells (T). Myeloid MM (indifferently MDM and MG cells) and PMN cells were strongly linked to the high IRE1 activity gene signature whereas T cells were not (**Fig.1A, S1A-B**). Using flow cytometry, we confirmed the presence of both myeloid populations in freshly dissociated samples from an in-house GB cohort (n=82) by quantifying expression of specific markers for each cell type (**Fig.1B-C, S1C-F**). Immune cell infiltration was higher in GB compared to grade II and III gliomas (**Fig.1B**), in particular CD45+ cells expressing MM and PMN markers (**Fig.1C, S1F**). MM constituted a majority of GB infiltrates[16], PMN were found in approximately 20% of the specimens, and T cell infiltration was rare (below 10%) (**Fig.1C**). Remarkably, infiltration of immune cells was higher in tumors with high IRE1 activity (**Fig.1D**), including CD11b positive cells expressing MM markers CD14, CD64 (specific for MDM/MMG) and CD163 (specific for MDM); and PMN markers CD15 and CD66b (**Fig.1E**). Again, T cell recruitment was not dependent on IRE1 activity (**Fig.1E**). This suggests that IRE1 signaling could contribute to myeloid attraction, which in turn may promote tumor aggressiveness. To test this hypothesis, monocytes and neutrophils attraction was assessed *in vitro*. Myeloid cells from healthy donors' blood, including monocytes (Mo) and PMN, were characterized based on the expression of CD14, CD15, CD66b and CD16 (**Fig.S1G**). In addition, we generated the RADH87 line stably overexpressing wild-type (WT) IRE1 or the truncated IRE1 variant, Q780* which is devoid of its kinase and RNase domains (**Fig.S1H-I**). The latter mutation attenuated IRE1 signaling (**Fig.S1J**), therefore resembling the characteristics of U87 DN cells which are deficient for IRE1 activation[10]. As shown in **Fig.1F-**

G, conditioned media derived from U87 DN and RADH87 Q780* did not recapitulate the migratory abilities of Mo and PMN in the Boyden chamber assay, when compared to conditioned media from parental U87 and RADH87 cells or RADH87 IRE1 WT cells. Thus, IRE1 activation in GB cells promotes PMN and Mo chemotaxis. Lastly, we evaluated the role of IRE1 activity in myeloid recruitment *in vivo* using two syngeneic GB mouse models. As such, mice were orthotopically injected with GL261 cells. Fourteen days later, mice underwent surgical tumor removal, followed by insertion of either an empty gel implant (CTR) or an implant containing the IRE1 RNase inhibitor, MKC8866 (MKC)[5,9]. Tumor size and overall survival obtained in both CTR and MKC groups were similar[9]. We showed that pharmacological abrogation of IRE1 activity by MKC8866 significantly reduced PMN infiltration in the recurring tumors mainly at the tumor core (**Fig.1H-I**) and led to increased MM recruitment at the tumor periphery (**Fig.S1K**). Additionally, mice were orthotopically injected with CT2A cells and treated with a novel IRE1 inhibitor B2-1, derived from the IRE1 inhibitor Z4P[17], that crosses the brain blood barrier[18]. Again, groups of CTR and B2-1 treated mice displayed similar tumor sizes and overall survival. However, the massive MM recruitment found in the CTR group was reduced upon IRE1 inhibition, similar to what was observed with PMN (**Fig.1H-I**). Overall, our results demonstrate that GB are infiltrated by myeloid cells, a phenomenon partly mediated by IRE1 signaling in tumor cells.

IRE1 activity regulates expression of myeloid-attracting chemokines

We next hypothesized that IRE1 activity in tumor cells controls expression of myeloid-attracting chemokines. The latter have been described in different cancer models and include CXCL1, CXCL2, CXCL5, CXCL7, IL6, and IL8 for PMN[19] and CCL2, CCL3, CCL5, CCL8, IL6 and IL8 for MM[20]. Using the TCGA dataset, we demonstrated that tumors with high IRE1 activity expressed high mRNA levels of the aforementioned cytokines/chemokines (**Fig.2A**). IRE1-dependent modulation of CXCL2, CXCL5, IL6 and IL8 was expected as these are part of the IRE1 activity signature[10]. Increased mRNA expression of these cytokines/chemokines in tumors correlated with higher expression of CD14 and CD15/CD16, markers for MM and

PMN, respectively (**Fig.2B, S2A**). To test whether those soluble factors promoted myeloid recruitment to GB, freshly isolated Mo and PMN were exposed to media conditioned by various GB lines, which resulted in significant induction of myeloid migration (**Fig.2C**). Using ELISA, we found that myeloid chemoattraction was correlated with elevated levels of CXCL2, IL6 and IL8 in these conditioned media (**Fig.2C**). PMN (but not Mo) attraction was partially blocked by SB225002, an antagonist of the IL8 receptor CXCR2 (**Fig.2D**). In line with our previous work[8], we showed that expression of myeloid-attracting chemokines depended on IRE1 activity. Indeed, expression of CXCL2, IL6 and IL8 mRNA but not CCL2 was dramatically reduced in U87 DN and RADH87 Q780* cells when compared to control or IRE1 WT-overexpressing cells (**Fig.2E-F**). Intriguingly, none of these chemokines/cytokines are known direct targets of XBP1s[21], suggesting an indirect contribution of XBP1s to this process. These findings indicate that IRE1 signaling, possibly through an indirect role of XBP1s, promotes the expression of chemokines involved in myeloid infiltration of tumors.

IRE1/XBP1s/RIDD control myeloid infiltration to GB via NFκB and UBE2D3

Since the expression of the aforementioned proinflammatory chemokines is controlled by NFκB[22], we tested whether a NFκB signaling gene signature was associated with IRE1, XBP1s and RIDD signatures previously established[10] using the TCGA data. This revealed that both XBP1s and RIDD signaling were oppositely associated with elevated NFκB activation (**Fig.3A**). We also analyzed NFκB activation in IRE1 signaling deficient U87 DN cells compared to parental cells. The expression and phosphorylation of NFκB was lower in U87 DN cells compared to control (**Fig.S2B**), demonstrating a functional relationship between IRE1 signaling and NFκB. Next, we postulated that IRE1 through both XBP1s and RIDD could oppositely regulate molecular actors that control NFκB activation. We thus compared lists comprising XBP1s direct targets identified using ChIPseq[21] with RIDD targets described in[10]; and identified 28 genes (**Fig.3B**). Among them, expression of seven correlated (either positively or negatively) with the IRE1 signature and only three with XBP1s and RIDD

signatures in GB samples (**Fig.3B**). Additionally, expression of only one of them, namely the E2 ubiquitin-conjugating enzyme UBE2D3, showed a marked positive correlation with NFκB activation (**Fig.3C**). Using TCGA transcriptome and RNAseq datasets, we showed that UBE2D3 mRNA expression was significantly higher in tumors with high IRE1 and XBP1s activities (**Fig.3D**) and in tumors expressing XBP1s mRNA (**Fig.3E**); but remained unaffected in tumors with high RIDD activity (**Fig.3D**). We then focused our attention on UBE2D3 as it also contributes to IκB degradation, and thus NFκB activation[23,24]. Intriguingly, we did not observe any effect on UBE2D3 mRNA or protein expression upon transient IRE1 inhibition using MKC8866 (**Fig.S2C-D**) or siRNA targeting either IRE1 (**Fig.S2E**) or XBP1 (**Fig.3F-G, S2F-H**). In addition, no effect was observed when the IRE1 activator IXA4 was used (**Fig.S2C-D**). However, UBE2D3 expression was reduced when IRE1 activity was stably attenuated in dominant negative U87 and RADH87 cells (**Fig.3H**). The effect was reversed by overexpressing XBP1s ectopically in these IRE1-defective cells (**Fig.3I**). This indicates that XBP1s could act as a transcriptional activator of UBE2D3 expression. Using the MatInspector and TFBIND tools, we found multiple potential XBP1s binding sites within the human and mouse UBE2D3 promoter region (**Fig.3J, S2I**). Gel shift assays revealed two sites for XBP1s binding on the human (sites *h1* and *h3*, **Fig.3K-L**) and one on the mouse (site *m1*, **Fig.S2J**) UBE2D3 promoter regions. Remarkably, multiple bands presented slower mobilities corresponding to higher molecular weight entities, suggesting that XBP1s could be part of larger complexes. Both human and mouse sites on the UBE2D3 promoter are flanked by other transcription factors binding sites, some of which are known to associate with XBP1s (data not shown). These results suggest that UBE2D3 expression could be regulated by XBP1s. At this stage however, an indirect control of XBP1s on UBE2D3 transcription cannot be excluded and further investigations are needed.

Conversely, UBE2D3 mRNA expression was decreased upon ER stress and this was significantly reduced upon treatment with MKC8866 (**Fig.4A**), suggesting that UBE2D3 is also targeted by RIDD upon ER stress. UBE2D3 functions together with E3 ligases including

SYVN1[25]. Since SYVN1 was previously demonstrated to contribute to IRE1 stability[26], we asked whether UBE2D3 also contributes to IRE1 expression regulation. As such modulation of UBE2D3 expression using either ectopic overexpression or siRNA silencing respectively led to reduced or increased IRE1 expression, independent of ER stress (**Fig.4B**). Furthermore, SYVN1 contributed to UBE2D3-dependent IRE1 degradation as shown using SYVN1 siRNA silencing in UBE2D3-overexpressing cells (**Fig.4C**). Notably, in contrast to UBE2D3, SYVN1 expression was neither modulated by IRE1 activity (**Fig.S2K**) nor associated with NFκB signaling pathway (**Fig.S2L**). Taken together, these results suggest that (i) in a basal/chronic ER stress situation, a prolonged inhibition of IRE1 activity (which is achieved by stable IRE1 DN overexpression, but not by a transient knockdown of IRE1/XBP1 or a short-term MKC treatment *in vitro*) is required to counteract IRE1-XBP1s-driven expression of UBE2D3 and that (ii) upon acute ER stress induction, transient IRE1 inhibition by MKC is sufficient to repress IRE1-mediated (RIDD-dependent) decrease of UBE2D3 expression. Thus, IRE1 via XBP1s and RIDD tightly controls UBE2D3 expression which, in turn, regulates IRE1 stability through SYVN1 as a feed-back mechanism (**Fig.4D**).

Next, both XBP1s and RIDD signatures previously established[10] were applied to the GB TCGA datasets to test whether these IRE1 signaling branches were associated with immune cell signatures. Importantly, the XBP1s signature was strongly linked to MM (including MG and MDM), PMN but not T immune signatures (**Fig.S3A**). In contrast, only the PMN signature was associated with the RIDD branch (**Fig.S3A**). Furthermore, amongst the IRE1 high/XBP1s high group, RIDD activity had no effect on myeloid recruitment whereas PMN were positively regulated by XBP1s activity in the IRE1 high/RIDD high group (**Fig.S3B).** Taken together, these data suggest that XBP1s is the main responsible of IRE1-controlled GB infiltration by myeloid cells.

UBE2D3 cooperates with MIB1 to trigger NFκB proinflammatory response

To investigate how UBE2D3 modulates NFκB activation, we evaluated the impact of UBE2D3 overexpression in GB lines on the NFκB regulator IκB and on the subsequent activation of the NFκB pathway. UBE2D3 overexpression led to IκB degradation and concomitant increased phosphorylation of NFκB (**Fig.5A, S4A-D**). To identify the putative E3 ligase(s) involved in IκB degradation and/or NFκB activation as well as to investigate the global effect of UBE2D3 on protein ubiquitination in GB, we carried out a label-free quantitative MS/MS analysis using cells stably overexpressing UBE2D3 (**Fig.S5**). Details of this analysis are in the Supplemental Results. Among proteins modulated by UBE2D3 expression, we identified the E3 ligase MIB1, a known regulator of NFκB activation[27] and interactor with UBE2D3[28]. Therefore, we investigated whether MIB1 cooperates with UBE2D3 to trigger the degradation of IκB. We found that MIB1 silencing partially prevented the UBE2D3-mediated degradation of IκB protein (**Fig.5B**, **S6A-B**). However, MIB1 also controlled UBE2D3 directly as MIB1 silencing led to increased expression of both UBE2D3 mRNA (**Fig.S6C**) and protein (**Fig.5B, S6A**), suggesting a complex interaction between these molecules. Overall, these results suggest the existence of a signaling axis involving UBE2D3 and MIB1 that is sufficient to trigger the activation of NFκB-dependent proinflammatory response in GB (**Fig.5G**), and which needs to be further analyzed.

IRE1/UBE2D3 control myeloid recruitment to GB through NF*κ*B proinflammatory response

To further investigate the role of UBE2D3 in myeloid mediated immunity, we stratified the TCGA GB cohort according to UBE2D3 mRNA levels and tested mRNA expression of the main myeloid-attracting cytokines/chemokines. We demonstrated that tumors with high UBE2D3 expression levels also expressed significantly higher levels of CCL2, CXCL2, IL6 and IL8 mRNA (**Fig.5C**). Next, we evaluated the expression of myeloid-attracting chemokines by RT-qPCR in UBE2D3-overexpressing cells. This showed that CCL2, CXCL2, IL6 and IL8 expression was markedly induced upon UBE2D3 overexpression (**Fig.5D**). In addition,

treatment of U87 cells with the NFκB inhibitor JSH-23, which prevents NFκB activity, blunted the observed UBE2D3-dependent increase in CCL2 CXCL2, IL6 and IL8 mRNA expression (**Fig.5E**). We next found that MIB1 silencing partially prevented the UBE2D3-mediated upregulation of CCL2, CXCL2, IL6 and IL8 in UBE2D3-overexpressing cells compared to control (**Fig.S6D**). Finally, we analyzed Mo and PMN attraction properties of conditioned media from GB cells modified for UBE2D3 expression. We confirmed that media conditioned by UBE2D3-overexpressing cells increased Mo and PMN migration compared with media conditioned by control cells (**Fig.5F**), which was partially reversed after blocking IL6 and IL8 with antibodies (**Fig.S6E**). In contrast, UBE2D3 down-regulation decreased Mo and PMN migration compared to control siRNA (siGL2) (**Fig.S6F**), and this effect was abolished by adding exogenously IL6 and IL8 (**Fig.S6G**). As expected, both cytokines were involved in Mo attraction, whereas only IL8 impacted PMN attraction (**Fig.S6E-G**), a result consistent with those presented in **Fig.2D**. In addition, Mo and PMN migration was reduced with media conditioned by UBE2D3 expressing RADH87 cells after MIB1 silencing, and this was reversed with exogenous IL6 and IL8 (**Fig.S6H**). Hence, we demonstrate that the signaling circuit involving IRE1/UBE2D3/MIB1 controls NFκB-mediated chemokines synthesis and inflammatory response in GB (**Fig.5G**).

UBE2D3 promotes pro-tumoral inflammation *in vivo* and increases GB aggressiveness

To assess the importance of IRE1/UBE2D3 signaling axis in GB, we used a syngeneic mouse model[9]. GL261 control and UBE2D3 overexpressing cells (**Fig.6A**) were orthotopically injected in immunocompetent C57BL/6 mice. Twenty-four days post-injection, tumors were resected, subjected to immunohistochemical analyses and the immune infiltrate was quantified. Interestingly, UBE2D3 GL261 cells produced larger tumors than their control counterparts (**Fig.6B**), although did not impact on mouse survival. This difference was not attributed to difference in proliferation rates *in vitro* (**Fig.S7A**), which suggests that the growth advantage of UBE2D3-overexpressing tumors might emerge from interaction with stroma

and/or tumor microenvironment. Accordingly, UBE2D3 tumors showed elevated NFκB expression (**Fig.6C**) and recruited significantly higher numbers of MM and PMN (**Fig.6D-E**), consistent with our *in vitro* findings. Furthermore, in UBE2D3-overexpressing cells, ccl2 and cxcl2 mRNA levels were increased, as well as other NFκB-dependent factors including g-csf, il1b and lif mRNA (**Fig.S7B**). Conditioned media from these cells also triggered Mo and PMN increased migration *in vitro* in a xenogeneic setting (**Fig.S7C**). Importantly, when ube2d3 was silenced in GL261 cells (**Fig.6F**), resulting tumors were smaller (**Fig.6G**), and mouse survival was extended compared to control cells (**Fig.6H**). Again, ube2d3 modulation did not influence GL261 proliferation *in vitro* (**Fig.S7D**), but affected mRNA expression of ccl2, cxcl2 as well as the factors under the control of NFκB activity i.e. g-csf, il1b and lif mRNA (**Fig.S7E**). Furthermore, conditioned media from GL261 shube2d3 cells were less efficient to promote Mo and PMN attraction *in vitro* (**Fig.S7F**). Since mice lack both *il8* and *il8 receptor (cxcr1)* genes, the PMN recruitment observed in our models could be due to cxcl1 and cxcl2, as previously reported in other mouse-bearing tumors infiltrated by PMN[29,30]. Using transcriptome data from two independent GB cohorts, GBMmark and TCGA-GBLGG, we observed a strong correlation between UBE2D3 expression and that of a large number of proinflammatory cytokines/chemokines (**Fig.S7G-H**). Intriguingly, high UBE2D3 expression was also associated with increased infiltration of monocytes, T cells and M2-polarized macrophages (**Fig.S7I-J**). Finally, to evaluate the clinical and prognostic relevance of UBE2D3 expression in GB, we investigated UBE2D3 expression in brain malignancies and showed that UBE2D3 was markedly increased in GB specimens compared to low-grade gliomas (**Fig.6I**). Patients whose tumors displayed high UBE2D3 expression were found associated with poorer prognosis, consistent with the fact that high IRE1 activity status was also of poor prognosis (**Fig.6I**). Our findings unveil a novel IRE1-dependent mechanism promoting pro-tumoral inflammation that integrates UPR signaling and ubiquitin system. Here, we demonstrated that IRE1/UBE2D3 axis controls GB secretome composition through NFκB signaling activation (**Fig.6J**).

Discussion

In recent years, we have characterized the relevance of UPR signaling, in particular of the IRE1 arm, in GB[7,8] and found that characteristics of IRE1 signaling represent a predictive factor for GB aggressiveness[10]. As such, modulating ER stress signaling pathways represents an attractive therapeutic avenue for GB treatment aimed at either increasing ER stress to levels that trigger apoptosis or decreasing the adaptive UPR, leading to loss of cellular selective advantages or increased sensitivity to treatments, and subsequent death[31]. In addition to the intrinsic aggressiveness of GB cells, the brain tumor microenvironment, which contains among others endothelial and immune cells, is emerging as a crucial regulator of cancer progression. The most abundant immune cells in GB microenvironment are tumor-associated macrophages and microglial cells that might reach up to 30% of the tumor mass and are often linked to disease aggressiveness[32,33]. However, brain tumors are also infiltrated by other immune cells such as T, myeloid and plasmacytoid DCs, and neutrophils[34].

In the present study, we demonstrated that IRE1 signaling in tumor cells plays a key role in regulating the GB microenvironment, by promoting myeloid recruitment to the tumors. We previously found that IRE1 signaling was involved in macrophages and microglial cells recruitment to the tumors[10] and that IRE1 controls proinflammatory chemokines expression[5,35]. Herein, we showed that pharmacological inhibition of IRE1 signaling decreased the extent of PMN infiltration into GB *in vivo* (**Fig.1**), which might be of clinical importance because elevated PMN recruitment correlated with poor outcome in GB patients. We also found that IRE1 activation in tumor cells was correlated with higher expression of myeloid-attracting chemokines (**Fig.2**). Importantly, this occurred in the absence of ER stress induction, underlining the important function of constitutive IRE1 activity in GB cells, i.e. modulating tumor secretome composition.

Mechanistically, we showed that IRE1 tightly and oppositely controlled the expression of UBE2D3 in GB cells by engaging the XBP1s and RIDD branches (**Fig.3, 4**). This result might be indicative of a stress-dependent (nature, time, intensity) regulation of UBE2D3 expression which could in turn find some spatial relevance in the whole tumor. We found that

activation of IRE1/UBE2D3 signaling axis was in part responsible for myeloid chemoattraction through NFκB activation (**Fig.5**). UBE2D3 is a E2 ubiquitin-conjugating enzyme that, together with E1 ubiquitin-activating enzyme and E3 ligase, mediates attachment of ubiquitin moieties to target proteins. This post-translational modification affects a broad range of biological processes, including protein quality control, trafficking, differentiation, cell division, signal transduction as well as inflammation[36,37]. UBE2D3 has been shown to control proteasomal degradation of, among others, p53[38], cyclin D1[39], p12 subunit of DNA polymerase δ[40] and IκBα[23,41]. It was also reported to mediate RIG-I ubiquitination and thereby promote its activation upon viral infection to initiate a type I interferon-dependent innate immune response[42]. In this study, we further demonstrated the crucial role of UBE2D3 in immunity/inflammation regulation in pathological conditions, such as cancer. We found that UBE2D3 is overexpressed in GB compared to low-grade gliomas, and that its elevated expression correlates with a high abundance of proinflammatory molecules. We delineated a novel IRE1-dependent mechanism for NFκB activation, which involves upregulation of UBE2D3 leading to IκB degradation through, at least partially, the E3 ligase MIB1 activity (**Fig.5**), the subsequent nuclear translocation of NFκB and its downstream signaling activation. Hence, IRE1 controls proinflammatory chemokines synthesis, including CXCL2, IL6 and IL8. as demonstrated herein. Once secreted, they not only sustain the pro-tumoral inflammatory microenvironment but can also mobilize immune cells recruitment to tumor sites further promoting cancer progression. As such, we showed *in vivo* that UBE2D3-overexpressing tumors were bigger in size and were infiltrated by significantly higher numbers of immune cells, such as MM and PMN (**Fig.6**). Furthermore, reduction of UBE2D3 led to decreased tumor growth *in vivo* and to the subsequent increased mouse survival. However, our findings indicate that the aforementioned mechanism might be applicable to the infiltration by a large number of lymphocytes, highlighting the importance of understanding the IRE1/UBE2D3 axis in other cancer models, particularly in 'immune hot' tumors. Recent studies using single-cell technologies reveal a large range of transcriptome phenotypes from myeloid

cells including both MDM and MG cells in GB[13–15]. The multidimensional heterogeneity of these myeloid populations (i.e. resting, repressed MG, primed MDM) renders complex their identification and studies[43,44]. Notably, IRE1 is involved in macrophage polarization in melanoma[45]. Whether and how IRE1 could be involved in controlling MDM/MG cell states and/or functions has to be further studied. Furthermore, the cross-talk between myeloid cells might determine GB cell fate and nature i.e., pro-neural to mesenchymal transition[46].

In the context of those findings, immunotherapy which has clearly proven its efficacy as an anti-cancer treatment[47,48], has so far led to disappointing results in GB, likely because of the powerful immunosuppressive features of those tumors[48]. Neutrophil-activating therapy is emerging as a powerful anti-cancer immunotherapeutic approach in mouse breast, colon and melanoma models[49]. Specific PMN activators including TNF, agonistic anti-CD40 and anti-tumor antibodies allow the PMN recruitment at metastatic sites and activate PMN-mediated antibody-dependent cytotoxicity against tumor cells. The current work implies that targeting IRE1 signaling might impede GB aggressiveness by reducing tumor cell invasion and angiogenesis[8,10], but also by attenuating pro-tumoral inflammation and immunity. This study opens a new avenue for therapeutic approaches to improve the efficacy of current and future immunotherapies.

Funding

This work was funded by grants from la Ligue Contre le Cancer, from INSERM, from Région Bretagne and from INCR to AT; from INSERM (IRP 2020 Tupric), Institut National du Cancer (INCa; PLBio 2017, 2019, 2020), Région Bretagne, Rennes Métropole, Fondation pour la recherche Médicale (FRM; équipe labellisée 2018 and DEQ20180339169), EU H2020 MSCA ITN-675448 (TRAINERS), la Ligue Contre le Cancer Comités d'Ille-et-Vilaine, des Côtes d'Armor et du Morbihan and MSCA RISE-734749 (INSPIRED) to EC; ELIXIR-GR "The Hellenic infrastructure for biological data management and analysis" (MIS: 5002780), "Reinforcement of the Research and Innovation Infrastructure", and the Operational Programme "Competitiveness, Entrepreneurship and Innovation" (NSRF 2014-2020) co-financed by Greece and the European Union (European Regional Development Fund) to AC.

Data Availability Statement

Materials described in the manuscript, including all relevant raw data, are freely available to any researcher wishing to use them for non-commercial purposes, without breaching participant confidentiality.

References

1. Chevet E, Hetz C, Samali A. Endoplasmic Reticulum Stress-Activated Cell Reprogramming in Oncogenesis. *Cancer discovery*. 2015;5(6):586-597. doi:10.1158/2159-8290.CD-14-1490
2. Almanza A, Carlesso A, Chintha C, et al. Endoplasmic reticulum stress signalling - from basic mechanisms to clinical applications. *The FEBS journal*. Published online July 20, 2018. doi:10.1111/febs.14608
3. Maurel M, Chevet E, Tavernier J, Gerlo S. Getting RIDD of RNA: IRE1 in cell fate regulation. *Trends in biochemical sciences*. 2014;39(5):245-254. doi:10.1016/j.tibs.2014.02.008 10.1016/j.tibs.2014.02.008. Epub 2014 Mar 20.
4. Urra H, Dufey E, Avril T, Chevet E, Hetz C. Endoplasmic Reticulum Stress and the Hallmarks of Cancer. *Trends Cancer*. 2016;2(5):252-262. doi:10.1016/j.trecan.2016.03.007
5. Logue SE, McGrath EP, Cleary P, et al. Inhibition of IRE1 RNase activity modulates the tumor cell secretome and enhances response to chemotherapy. *Nature communications*. 2018;9(1):3267. doi:10.1038/s41467-018-05763-8
6. Obacz J, Avril T, Rubio-Patiño C, et al. Regulation of tumor-stroma interactions by the unfolded protein response. *FEBS J*. 2019;286(2):279-296. doi:10.1111/febs.14359
7. Dejeans N, Pluquet O, Lhomond S, et al. Autocrine control of glioma cells adhesion and migration through IRE1alpha-mediated cleavage of SPARC mRNA. *Journal of cell science*. 2012;125(Pt 18):4278-4287. doi:jcs.099291 [pii]10.1242/jcs.099291 10.1242/jcs.099291. Epub 2012 Jun 20.
8. Auf G, Jabouille A, Guerit S, et al. Inositol-requiring enzyme 1alpha is a key regulator of angiogenesis and invasion in malignant glioma. *Proceedings of the National Academy of Sciences of the United States of America*. 2010;107(35):15553-15558. doi:10.1073/pnas.0914072107
9. Le Reste PJ, Pineau R, Voutetakis K, et al. Local intracerebral inhibition of IRE1 by MKC8866 sensitizes glioblastoma to irradiation/chemotherapy in vivo. *Cancer Lett*. 2020;494:73-83. doi:10.1016/j.canlet.2020.08.028
10. Lhomond S, Avril T, Dejeans N, et al. Dual IRE1 RNase functions dictate glioblastoma development. *EMBO molecular medicine*. Published online January 8, 2018. doi:10.15252/emmm.201707929
11. Hu P, Han Z, Couvillon AD, Kaufman RJ, Exton JH. Autocrine tumor necrosis factor alpha links endoplasmic reticulum stress to the membrane death receptor pathway through IRE1alpha-mediated NF-kappaB activation and down-regulation of TRAF2 expression. *Molecular and cellular biology*. 2006;26(8):3071-3084.
12. Avril T, Vauleon E, Hamlat A, et al. Human glioblastoma stem-like cells are more sensitive to allogeneic NK and T cell-mediated killing compared with serum-cultured glioblastoma cells. *Brain pathology*. 2012;22(2):159-174. doi:10.1111/j.1750-3639.2011.00515.x
13. Yin W, Ping YF, Li F, et al. A map of the spatial distribution and tumour-associated macrophage states in glioblastoma and grade-4 IDH-mutant astrocytoma. *J Pathol*. Published online June 20, 2022. doi:10.1002/path.5984
14. Bowman RL, Klemm F, Akkari L, et al. Macrophage Ontogeny Underlies Differences in Tumor-Specific Education in Brain Malignancies. *Cell Rep*. 2016;17(9):2445-2459. doi:10.1016/j.celrep.2016.10.052
15. Cui X, Wang Q, Zhou J, et al. Single-Cell Transcriptomics of Glioblastoma Reveals a Unique Tumor Microenvironment and Potential Immunotherapeutic Target Against Tumor-Associated Macrophage. *Front Oncol*. 2021;11:710695. doi:10.3389/fonc.2021.710695
16. Badie B, Schartner JM. Flow cytometric characterization of tumor-associated

macrophages in experimental gliomas. *Neurosurgery*. 2000;46(4):957-961; discussion 961-2.
17. Pelizzari-Raymundo D, Doultsinos D, Pineau R, et al. A novel IRE1 kinase inhibitor for adjuvant glioblastoma treatment. *iScience*. 2023;26(5):106687. doi:10.1016/j.isci.2023.106687
18. Chevet E, Doultsinos D, Eriksson L a, et al. Compounds Containing a Hydroxyphenyl Moiety and Their Use. 2023;(EP22305014A·2022-01-07).
19. Powell DR, Huttenlocher A. Neutrophils in the Tumor Microenvironment. *Trends in immunology*. 2016;37(1):41-52. doi:10.1016/j.it.2015.11.008
20. Guedes JR, Lao T, Cardoso AL, El Khoury J. Roles of Microglial and Monocyte Chemokines and Their Receptors in Regulating Alzheimer's Disease-Associated Amyloid-beta and Tau Pathologies. *Front Neurol*. 2018;9:549. doi:10.3389/fneur.2018.00549
21. Chen X, Iliopoulos D, Zhang Q, et al. XBP1 promotes triple-negative breast cancer by controlling the HIF1alpha pathway. *Nature*. 2014;508(7494):103-107. doi:10.1038/nature13119
22. Richmond A. Nf-kappa B, chemokine gene transcription and tumour growth. *Nat Rev Immunol*. 2002;2(9):664-674. doi:10.1038/nri887
23. Yaron A, Hatzubai A, Davis M, et al. Identification of the receptor component of the IkappaBalpha-ubiquitin ligase. *Nature*. 1998;396(6711):590-594. doi:10.1038/25159
24. Gonen H, Bercovich B, Orian A, et al. Identification of the ubiquitin carrier proteins, E2s, involved in signal-induced conjugation and subsequent degradation of IkappaBalpha. *The Journal of biological chemistry*. 1999;274(21):14823-14830. doi:10.1074/jbc.274.21.14823
25. Nadav E, Shmueli A, Barr H, Gonen H, Ciechanover A, Reiss Y. A novel mammalian endoplasmic reticulum ubiquitin ligase homologous to the yeast Hrd1. *Biochem Biophys Res Commun*. 2003;303(1):91-97. doi:10.1016/s0006-291x(03)00279-1
26. Gao B, Lee SM, Chen A, et al. Synoviolin promotes IRE1 ubiquitination and degradation in synovial fibroblasts from mice with collagen-induced arthritis. *EMBO Rep*. 2008;9(5):480-485. doi:10.1038/embor.2008.37
27. Liu LJ, Liu TT, Ran Y, et al. The E3 ubiquitin ligase MIB1 negatively regulates basal IkappaBalpha level and modulates NF-kappaB activation. *Cell Res*. 2012;22(3):603-606. doi:10.1038/cr.2011.199
28. van Wijk SJ, de Vries SJ, Kemmeren P, et al. A comprehensive framework of E2-RING E3 interactions of the human ubiquitin-proteasome system. *Molecular systems biology*. 2009;5:295. doi:10.1038/msb.2009.55
29. Jablonska J, Wu CF, Andzinski L, Leschner S, Weiss S. CXCR2-mediated tumor-associated neutrophil recruitment is regulated by IFN-β. *International Journal of Cancer*. 2014;134(6):1346-1358. doi:10.1002/ijc.28551
30. Gershkovitz M, Fainsod-Levi T, Zelter T, Sionov RV, Granot Z. TRPM2 modulates neutrophil attraction to murine tumor cells by regulating CXCL2 expression. *Cancer Immunol Immunother*. 2019;68(1):33-43. doi:10.1007/s00262-018-2249-2
31. Obacz J, Avril T, Le Reste PJ, et al. Endoplasmic reticulum proteostasis in glioblastoma-From molecular mechanisms to therapeutic perspectives. *Sci Signal*. 2017;10(470):eaal2323. doi:10.1126/scisignal.aal2323
32. Hambardzumyan D, Gutmann DH, Kettenmann H. The role of microglia and macrophages in glioma maintenance and progression. *Nature neuroscience*. 2016;19(1):20-27. doi:10.1038/nn.4185
33. Bingle L, Brown NJ, Lewis CE. The role of tumour-associated macrophages in tumour progression: implications for new anticancer therapies. *The Journal of pathology*. 2002;196(3):254-265. doi:10.1002/path.1027
34. Quail DF, Joyce JA. The Microenvironmental Landscape of Brain Tumors. *Cancer*

cell. 2017;31(3):326-341. doi:10.1016/j.ccell.2017.02.009
35. Pluquet O, Dejeans N, Bouchecareilh M, et al. Posttranscriptional regulation of PER1 underlies the oncogenic function of IREalpha. *Cancer research*. 2013;73(15):4732-4743. doi:10.1158/0008-5472.CAN-12-3989
36. Mukhopadhyay D, Riezman H. Proteasome-independent functions of ubiquitin in endocytosis and signaling. *Science*. 2007;315(5809):201-205. doi:10.1126/science.1127085
37. Glickman MH, Ciechanover A. The ubiquitin-proteasome proteolytic pathway: destruction for the sake of construction. *Physiological reviews*. 2002;82(2):373-428. doi:10.1152/physrev.00027.2001
38. Saville MK, Sparks A, Xirodimas DP, et al. Regulation of p53 by the ubiquitin-conjugating enzymes UbcH5B/C in vivo. *The Journal of biological chemistry*. 2004;279(40):42169-42181. doi:10.1074/jbc.M403362200
39. Hattori H, Zhang X, Jia Y, et al. RNAi screen identifies UBE2D3 as a mediator of all-trans retinoic acid-induced cell growth arrest in human acute promyelocytic NB4 cells. *Blood*. 2007;110(2):640-650. doi:10.1182/blood-2006-11-059048
40. Zhang S, Zhou Y, Sarkeshik A, et al. Identification of RNF8 as a ubiquitin ligase involved in targeting the p12 subunit of DNA polymerase delta for degradation in response to DNA damage. *The Journal of biological chemistry*. 2013;288(5):2941-2950. doi:10.1074/jbc.M112.423392
41. Wu K, Kovacev J, Pan ZQ. Priming and extending: a UbcH5/Cdc34 E2 handoff mechanism for polyubiquitination on a SCF substrate. *Molecular cell*. 2010;37(6):784-796. doi:10.1016/j.molcel.2010.02.025
42. Shi Y, Yuan B, Zhu W, et al. Ube2D3 and Ube2N are essential for RIG-I-mediated MAVS aggregation in antiviral innate immunity. *Nature communications*. 2017;8:15138. doi:10.1038/ncomms15138
43. Yeo AT, Rawal S, Delcuze B, et al. Single-cell RNA sequencing reveals evolution of immune landscape during glioblastoma progression. *Nat Immunol*. 2022;23(6):971-984. doi:10.1038/s41590-022-01215-0
44. Arrieta VA, Najem H, Petrosyan E, et al. The Eclectic Nature of Glioma-Infiltrating Macrophages and Microglia. *Int J Mol Sci*. 2021;22(24):13382. doi:10.3390/ijms222413382
45. Batista A, Rodvold JJ, Xian S, et al. IRE1α regulates macrophage polarization, PD-L1 expression, and tumor survival. *PLOS Biology*. 2020;18(6):e3000687. doi:10.1371/journal.pbio.3000687
46. Chen Z, Soni N, Pinero G, et al. Monocyte depletion enhances neutrophil influx and proneural to mesenchymal transition in glioblastoma. *Nat Commun*. 2023;14(1):1839. doi:10.1038/s41467-023-37361-8
47. Ribas A, Wolchok JD. Cancer immunotherapy using checkpoint blockade. *Science*. 2018;359(6382):1350-1355. doi:10.1126/science.aar4060
48. Lim M, Xia Y, Bettegowda C, Weller M. Current state of immunotherapy for glioblastoma. *Nature reviews Clinical oncology*. 2018;15(7):422-442. doi:10.1038/s41571-018-0003-5
49. Linde IL, Prestwood TR, Qiu J, et al. Neutrophil-activating therapy for the treatment of cancer. *Cancer Cell*. 2023;41(2):356-372.e10. doi:10.1016/j.ccell.2023.01.002

Figure Legends

Figure 1. Impact of IRE1 on myeloid recruitment to GB *in vitro* and *in vivo*.

(A) Hierarchical clustering of TCGA GB patients based on high/low IRE1 activity was confronted to immune markers for MM, MDM, MG, PMN and T cells. UP (n) and *p* values denote the proportion of signature genes that were found up-regulated between the groups (n=number of genes) and the estimated two-sided directional *p*-value of test, respectively. **(B)** Total immune infiltrate of GB (n=82) and grade II/III (n=8/14) glioma analyzed by flow cytometry using anti-CD45 antibodies. (***): $p<0.001$ according to unpaired t-test compared to GB. **(C)** Percentage of specific GB infiltrated leukocytes populations analyzed by flow cytometry using anti-CD45/CD11b antibodies. Tumors were classified according to IRE1 activity (high/blue in red/blue) (n=31). **(D)** Total immune infiltrate of GB classified according to IRE1 activity (high/low in red/blue, n=14/7) and analyzed by flow cytometry using anti-CD45 antibodies. Tumors were classified using transcriptome analysis according to IRE1 signature. (***): $p<0.001$ according to unpaired t-test compared to tumors with high IRE1 activity. **(E)** Deeper characterization of immune subtypes was performed combining specific markers i.e. MM markers CD14, CD64 (for MDM/MMG), CD163 (for MDM), PMN markers CD15 and CD66B, and T marker CD3. Tumors were classified according to IRE1 activity (high/low, n=10/5). ns: not significant, (*): $p<0.05$ and (**): $p<0.01$ according to unpaired t-test compared to tumors with high IRE1 activity. **(F, G)** Freshly isolated Mo and PMN were placed in Boyden chambers towards fresh medium (-), conditioned media from U87 (par.), U87 DN (DN), RADH87 (par.), RADH87 cells overexpressing IRE1 (WT) or Q780* (Q*) (n=3, mean±SD). ns: not significant, (*): $p<0.05$, (**): $p<0.01$, (****): $p<0.0001$ according to unpaired t-test compared to media from parental. **(H)** Representative immunohistological analysis of myeloid infiltration in GB resected from GL261 and CT2A-implanted mice treated with plug with IRE1 inhibitor MKC8866 (for GL261) and B2-1 (for CT2A), respectively. MM and PMN were detected with anti-IBA1 and anti-Ly6G antibodies, respectively. Scale bar 100 µm. **(I)** Semi-quantitative analysis of IBA1 and Ly6G staining from (H). *p* values from unpaired t-test compared to CTR; ns: not significant.

Figure 2. IRE1-mediated synthesis of myeloid-attracting chemokines.

(A) Hierarchical clustering of TCGA GB patients based on high/low IRE1 activity (n=264/275) confronted to chemokines expression involved in myeloid chemoattraction. *p* values obtained using unpaired t-test comparing IRE1 high versus low tumors. **(B)** Chemokines mRNA expression in TCGA GB tumors with high/low (red/blue) MM and PMN infiltration determined according to CD14 or CD15 levels, respectively. CD14/CD15 high/low groups were determined using the median of the marker mRNA expression as cut-off (high/low n=263/263). *p* values according to unpaired t-test comparing chemokines mRNA expression between CD14/CD15 high versus low tumors. **(C)** Correlation between chemokines secretion and Mo/ PMN migration towards tumor conditioned media from different GB lines (n= 7 and 20 for Mo and PMN respectively). R square and *p* values of the slopes were calculated using Pearson correlation coefficient analysis between chemokines secretion and myeloid attraction; ns: not significant and (*): $p<0.05$. **(D)** Myeloid migration assay was performed as described in **Fig.1**, in the presence of SB225002, a CXCR2 antagonist (n=3 and 4 for Mo and PMN respectively, mean±SD). ns: not significant and (**): $p<0.01$ according to unpaired t-test compared to DMSO. **(E)** Quantification of myeloid-attracting chemokines mRNA abundance using RT-qPCR in parental U87 and RADH87 cells (-) transiently overexpressing TRAP-Nck (TRAP), IRE1-Nck (DN), IRE1-Q780* (Q) (n=4). *p* values according to an ANOVA test comparing the four conditions. **(F)** Quantification of chemokines mRNA expression using RT-qPCR in parental U87 (par.), U87 DN (stably overexpressing IRE1-Nck), parental RADH87 or RADH87 cells stably overexpressing wild-type (WT) or Q780* (Q*) IRE1 (n=at least 6, mean±SD). ns: not significant, (**): $p<0.01$, (***): $p<0.001$, (****): $p<0.0001$ according to unpaired t-test compared to parental.

Figure 3. IRE1/XBP1-dependent regulation of UBE2D3.

(A) IRE1, XBP1s and RIDD signatures were confronted to NFκB signaling gene signature using the TCGA GB dataset (IRE1 high/low n=264/275; XBP1s high/low n=261/210; and RIDD

high/low n=285/249). *p* values obtained with unpaired t-test comparing IRE1, XBP1s and RIDD high versus low tumors. **(B)** Venn diagram of the intersection of XBP1s target genes identified by ChIPseq [21] with RIDD targets [10]. **(C)** Association of NFκB signature with NCSTN, UBE2D3 and UFM1 low/high GB from TCGA. NCSTN, UBE2D3 and UFM1 high/low groups were determined using the median of the mRNA expression as cut-off (high/low n=263/263). *p* values obtained from unpaired t-test comparing NCSTN, UBE2D3 and UFM1 high versus low tumors. **(D)** UBE2D3 mRNA expression in TCGA GB categorized according to their IRE1, XBP1s and RIDD signatures (IRE1 high/low n=258/265; XBP1s high/low n=261/210; and RIDD high/low n=252/258). *p* values obtained with unpaired t-test comparing IRE1, XBP1s and RIDD high versus low tumors. **(E)** UBE2D3 mRNA expression in XBP1s low/high TCGA GB (RNAseq dataset; high/low n=80/86). *p* value obtained from unpaired t-test comparing XBP1s high versus low tumors. **(F)** Quantitation of UBE2D3 mRNA expression using RT-qPCR in U87 and RADH87 cells silenced for XBP1 (n=7 and 4 respectively for U87 and RADH87). ns: not significant according to unpaired t-test compared to control. **(G)** Western blot analysis of UBE2D3 in parental (NT), control (siCTR) and XBP1-silenced (siXBP1) U87 and RADH87 cells. Actin (ACT) was used as loading control. Data are representative of three biological replicates (see **Fig.S4F**). **(H)** Quantification of UBE2D3 mRNA expression by RT-qPCR in cells with active (parental U87 and RADH87 (par)) and inactive IRE1 signaling (U87 DN and RADH87 Q780*) (n=4, mean±SD). (*): $p<0.05$ according to unpaired t-test compared to parental. **(I)** Quantitation of UBE2D3 expression with RT-qPCR in U87 DN and RADH87 Q* cells and transfected with XBP1s (n=3). (*): $p<0.05$, (***): $p<0.001$ according to unpaired t-test comparing CTR to XBP1s conditions. **(J)** Putative XBP1s binding sites (green) on human UBE2D3 promoter regions analyzed with MatInspector and TFBIND. **(K-L)** Gel shift assays performed on 4 putative XBP1s binding sites using U87 nuclear extracts after XBP1s overexpression (K). Validation of putative binding sites *h1*, *h2* and *h3* using gradual amounts of unlabeled probes used in competition assay (L).

Figure 4. IRE1/RIDD-dependent regulation of UBE2D3.

(A) Western blot analysis of UBE2D3 in U87 cells treated with MKC8866 (MKC) under basal or ER stress condition using thapsigargin (Tg, 50 nM). *p* value obtained using an ANOVA test. **(B)** Western blot analysis of IRE1 and UBE2D3 in U87 cells silenced for UBE2D3 and UBE2D3 overexpressing RADH87 cells under basal or ER stress condition using tunicamycin (Tm, 1 µg/mL). **(C)** Western blot analysis of IRE1 and UBE2D3 in UBE2D3 overexpressing U87 cells silenced for SYVN1 under basal or ER stress condition using Tm. **(D)** Schematic representation of IRE1 regulation of UBE2D3 expression with a retro-control loop involving SYVN1.

Figure 5. Impact of UBE2D3 on NFκB activation and chemokines synthesis.

(A-B) Western blot analysis of NFκB, phospho-NFκB, IκB and phospho-IκB in control (EV) and transiently (U87) or stably (RADH87) UBE2D3 overexpressing cells (A); and after MIB1 down-regulation (siMIB1) (B). UBE2D3 over-expression was checked. **(C)** Chemokines mRNA expression in TCGA GB specimens categorized according to UBE2D3 expression. UBE2D3 high/low (red/blue, n=263/263) groups were determined using the median of the mRNA expression as cut-off. *p* values obtained from unpaired t-test comparing UBE2D3 high versus low tumors. **(D)** Quantification of chemokines expression using RT-qPCR in control (CTR) U87, parental (par.) RADH87, transient U87 and stable RADH87 cells overexpressing UBE2D3 (n=3, mean±SD). (*): $p<0.05$, (**): $p<0.01$, (***): $p<0.001$, (****): $p<0.0001$ according to unpaired t-test compared to control. **(E)** Quantification of chemokines expression using RT-qPCR in U87 (EV) or UBE2D3 overexpressing cells treated with 5 µM JSH-23 (n=3, mean±SD). (*): $p<0.05$, (**): $p<0.01$, (****): $p<0.0001$ according to unpaired t-test compared to control. **(F)** Myeloid migration (Mo and PMN) was performed as described in **Fig.1**, towards media conditioned by U87 control (CTR) and UBE2D3 overexpressing cells (n=3, mean±SD). (*): $p<0.05$ and (***): $p<0.001$ according to unpaired t-test compared to control. **(G)** Schematic representation of UBE2D3 impact on inflammatory response in GB.

Figure 6. Impact of UBE2D3 overexpression on inflammation *in vivo*.

(A) UBE2D3 protein overexpression in five UBE2D3 transfected GL261 stable lines. UBE2D3 protein level was measured with anti-Flag antibodies. **(B)** Left panel: brain sections from mice injected with GL261 control (CTR) or GL261_UBE2D3 cells analyzed for vimentin expression. Scale bar 1 mm. Right panel: tumor volume in control and UBE2D3 overexpressing (oe) group (n=3 and 10, mean±SD). ns: not significant according to unpaired t-test compared to control. **(C-E)** Left panel: Representative immunohistological NFκB expression (n=7/15, mean±SD) (C), macrophages/microglia infiltration (n=18, mean±SD) (D) and neutrophils infiltration (n=24, mean±SD) (E) in GL261 control or GL261_UBE2D3 tumors detected by anti-NFκB, anti-IBA1 and anti-Ly6G antibodies, respectively. Scale bar 100 µm. Right panel: semi-quantitative analyses of NFκB (C), IBA1 (D) and Ly6G staining (E) in control and GL261_UBE2D3 tumors. (*):$p<0.05$, (**):$p<0.01$ according to unpaired t-test compared to control. **(F)** UBE2D3 protein silencing in two GL261 stable lines transfected with shube2d3 construct. UBE2D3 protein level was measured using anti-ube2d3 antibodies. **(G)** Left panel: brain sections from mice injected with GL261 shCTR or shube2d3 GL261 cells analyzed for vimentin expression. Scale bar 1 mm. Right panel: tumor volume in shCTR and shube2d3 group (n=4, mean±SD). (*): $p<0.05$ according to unpaired t-test comparing to control. **(H)** Mouse survival of mouse bearing parental, shCTR and shube2d3 GL261 cells. (***): $p<0.001$ according to unpaired t-test comparing to parental. **(I)** UBE2D3 expression in LGG and GB (mean; *p* value according to unpaired t-test compared to GB); and its impact on patients' survival. **(J)** Schematic representation of IRE1/UBE2D3 axis in the regulation of pro-tumoral inflammation.

Figure 1

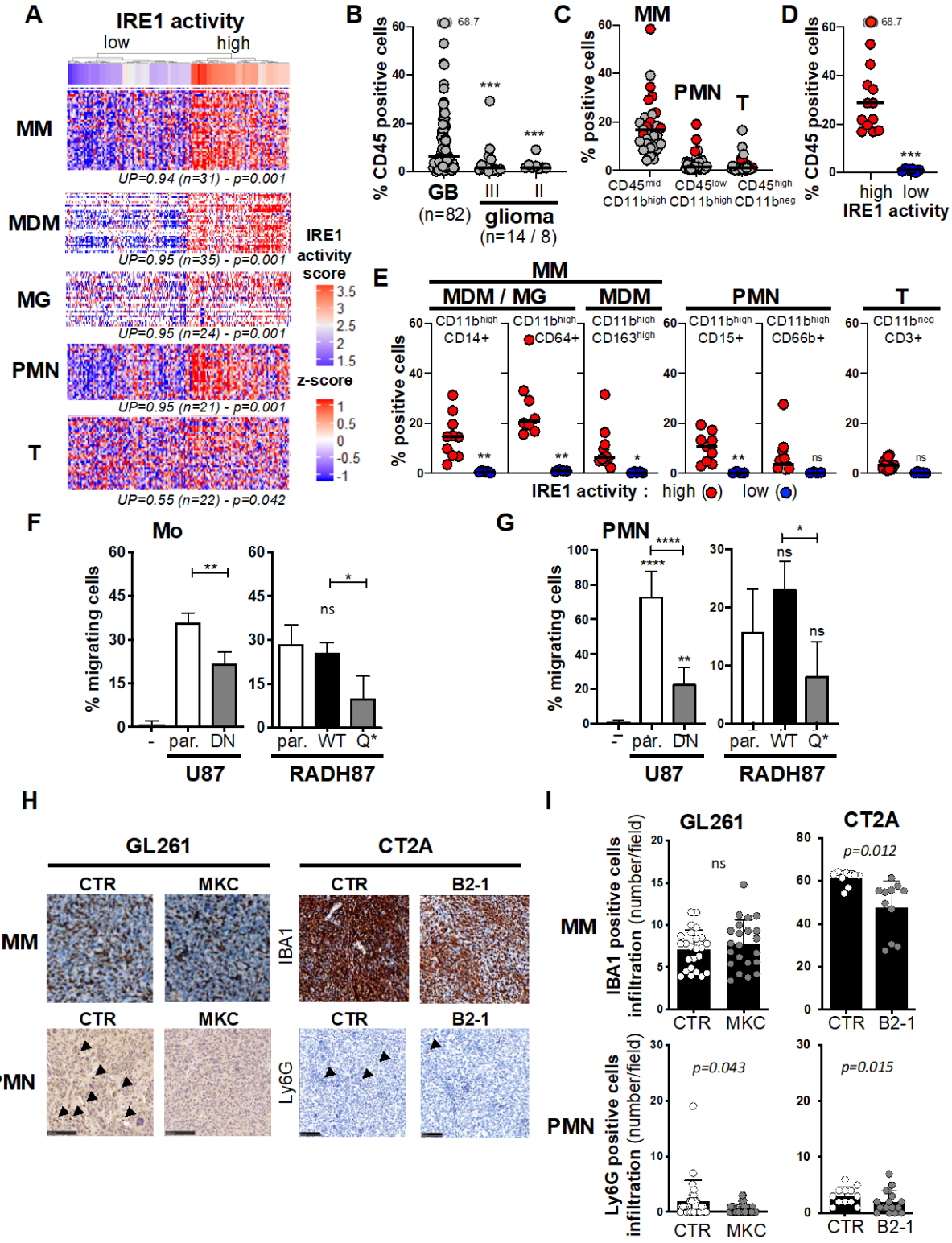

1

Figure 2

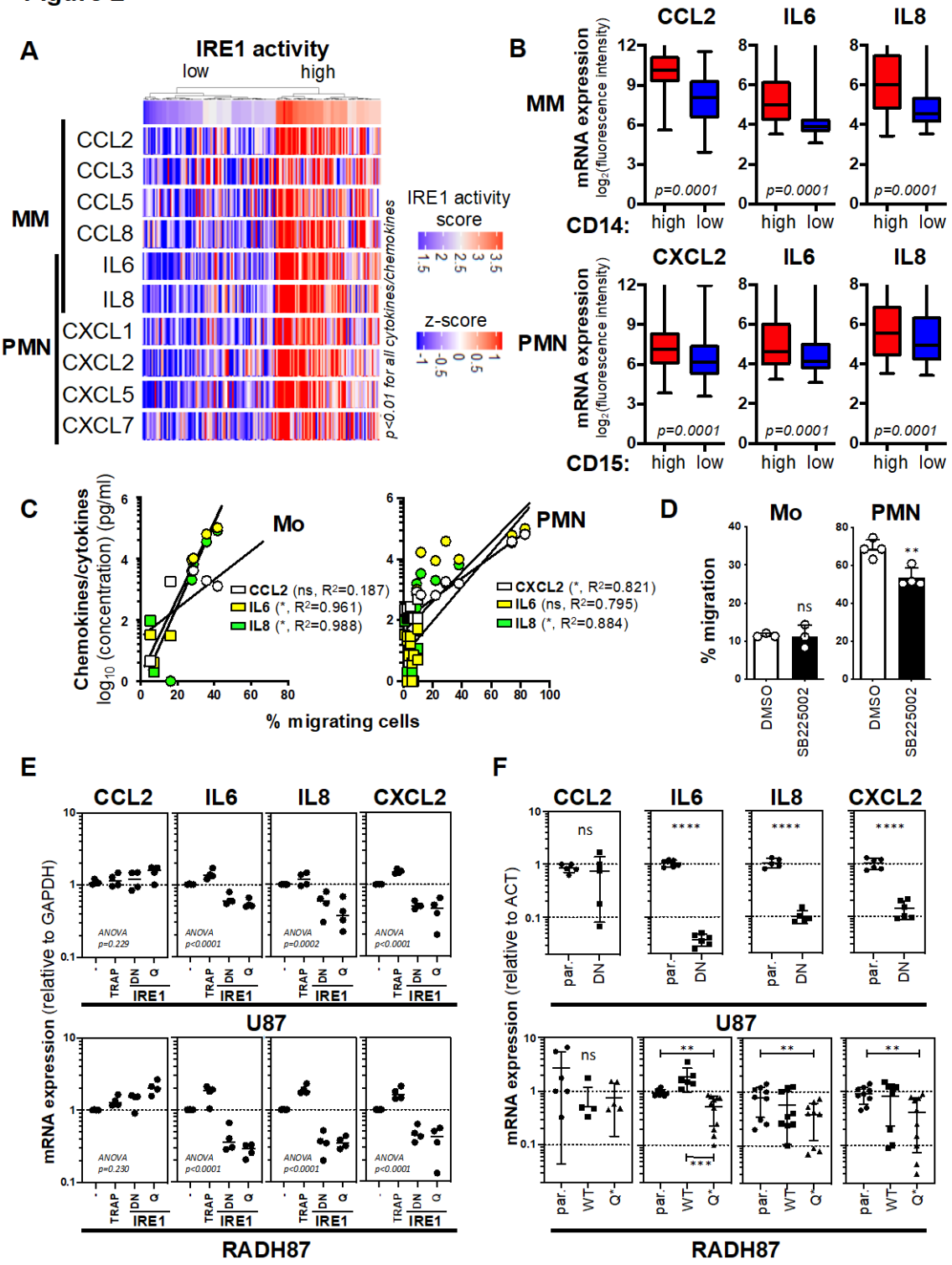

1

Figure 3

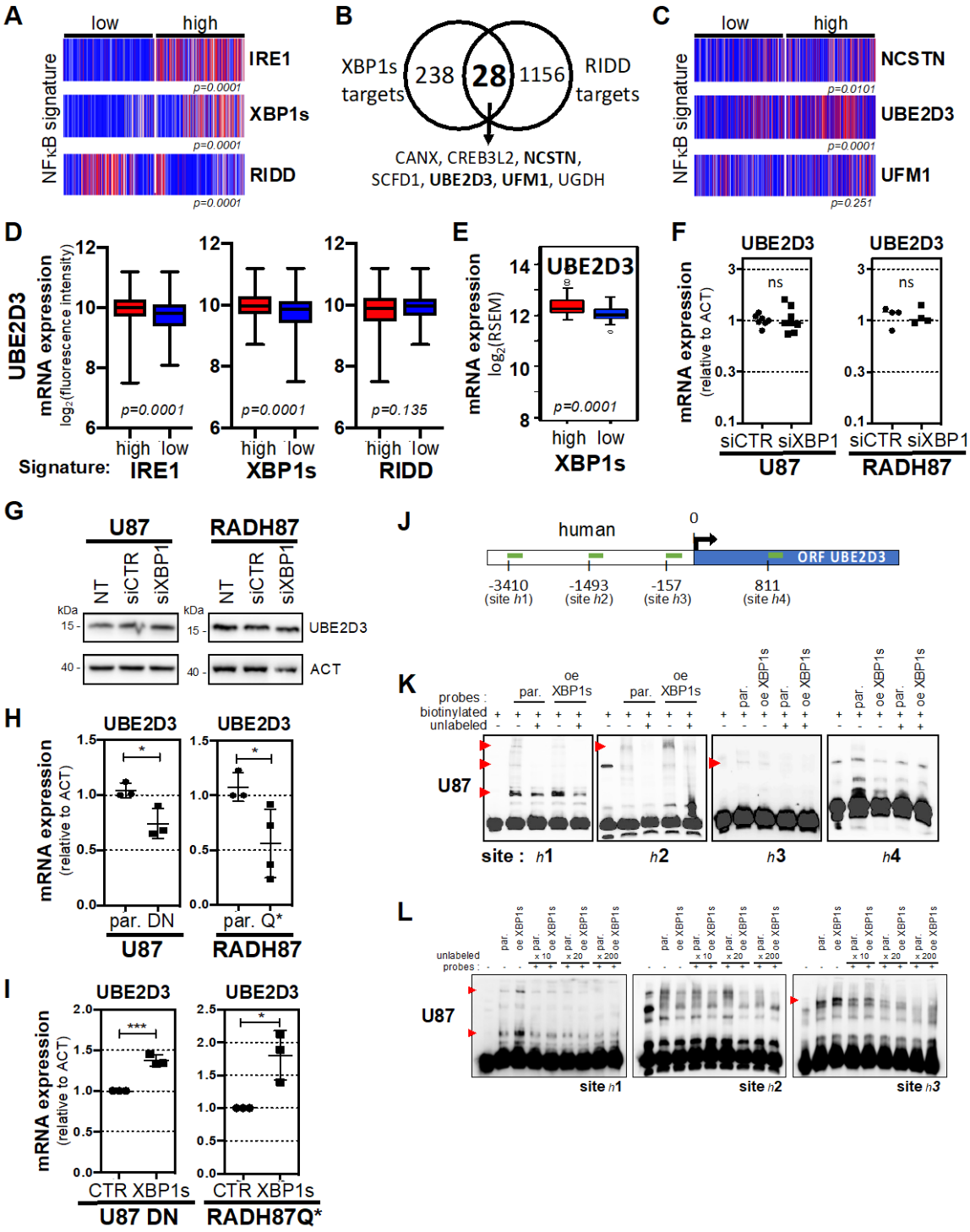

1

Figure 4

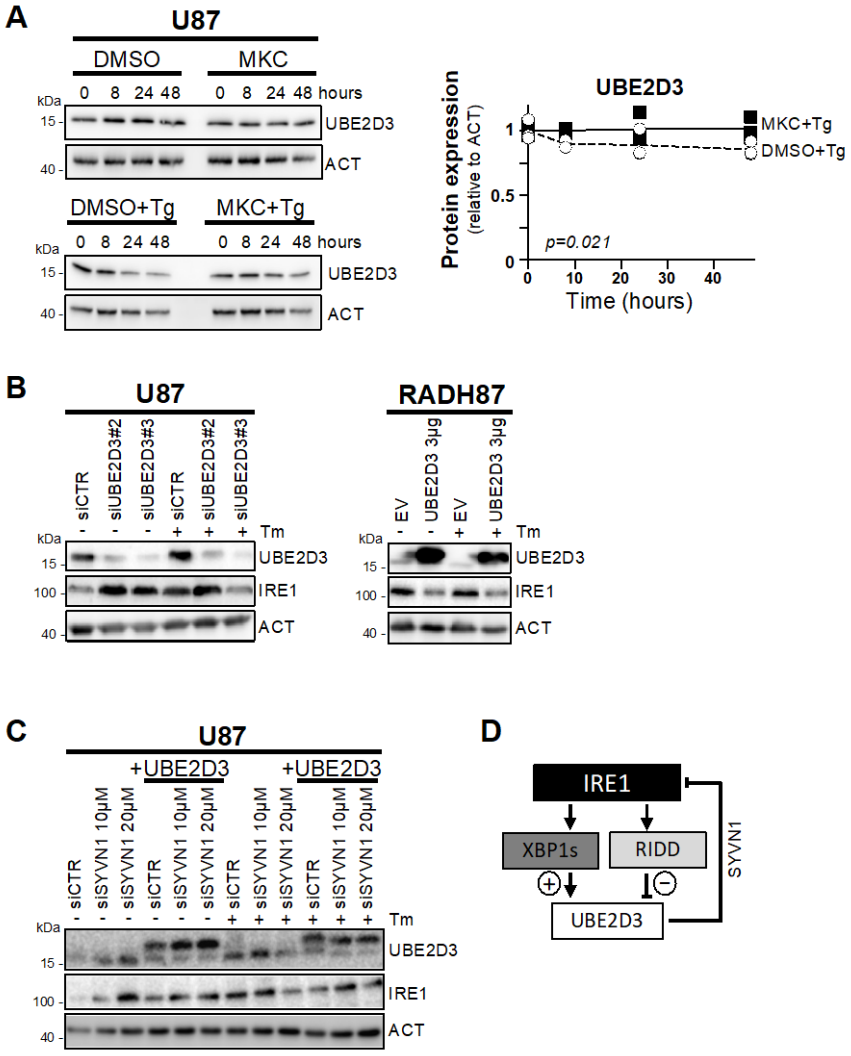

1

Figure 5

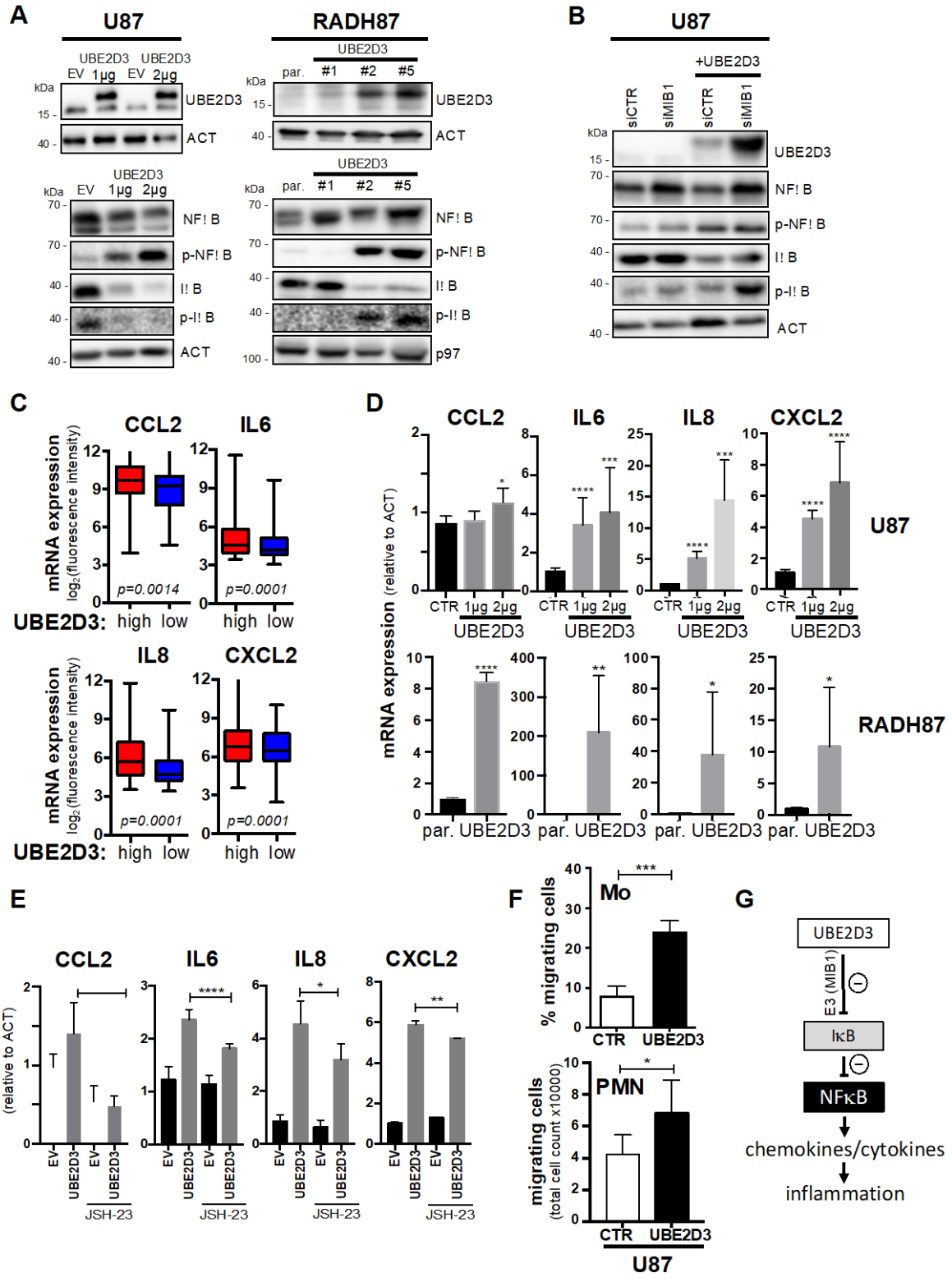

1

Figure 6

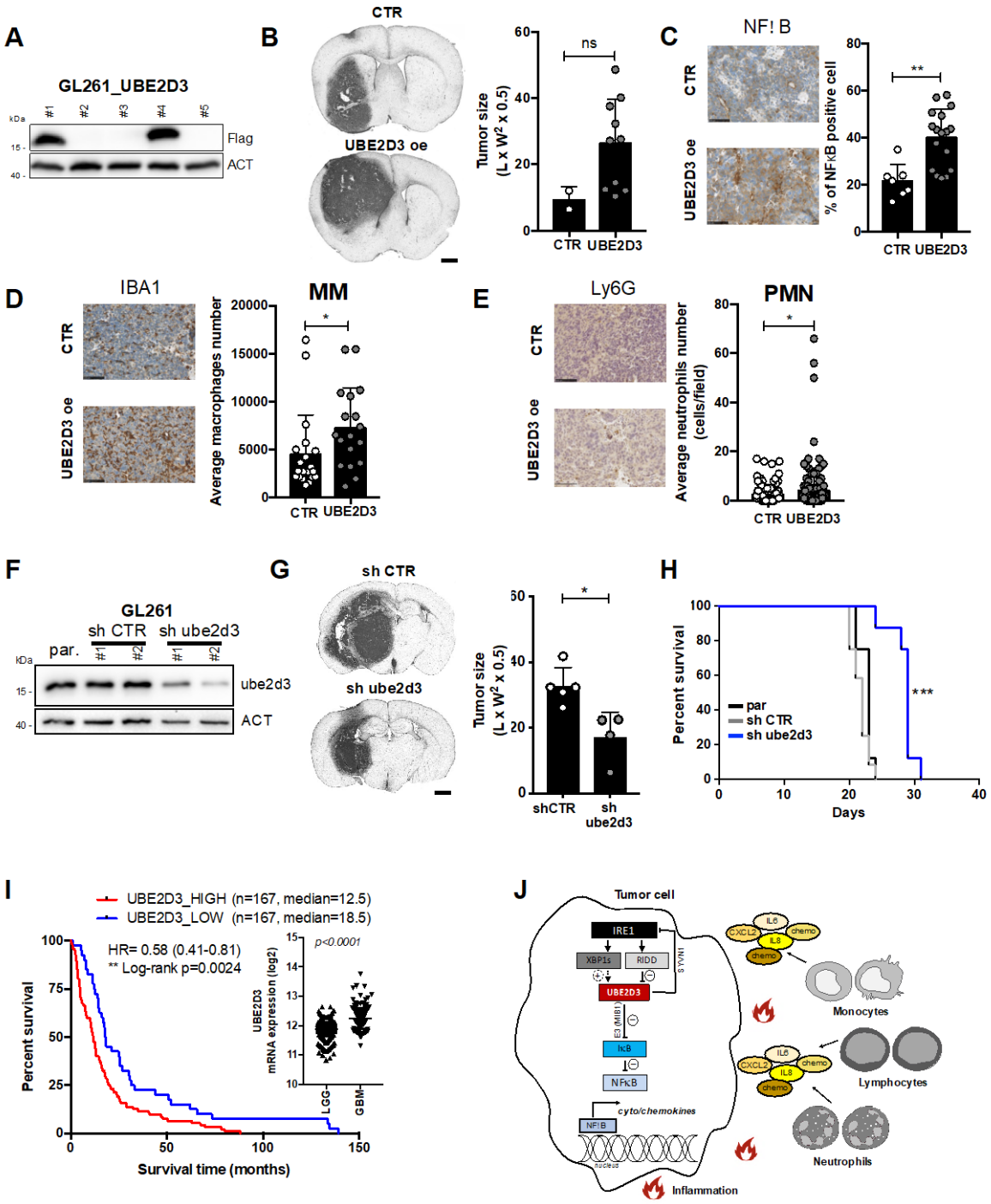

1